Global Journal of Pure and Applied Mathematics.
ISSN 0973-1768 Volume 11, Number 1 (2015), pp. 537–556

http://www.ripublication.com

Double diffusive natural convection in a partially permeable rectangular cavity heated from below

Neetu Srivastava and Ashok K. Singh

Department of Mathematics, Faculty of Science,
Banaras Hindu University, Varanasi – 221005, India.
E-mail: neetusrivastava81@gmail.com; ashok@bhu.ac.in

Pallath Chandran[1] **and Nirmal C. Sacheti**

Department of Mathematics and Statistics,
College of Science, Sultan Qaboos University,
PC 123, Al Khod, Muscat, Sultanate of Oman
E-mail: chandran@squ.edu.om; nirmal@squ.edu.om

Abstract

Simultaneous heat and mass transfer in a composite system comprising a viscous fluid layer overlying a porous layer saturated with the same fluid has been investigated. The horizontal walls of the cavity are assumed to be heated from below and cooled from above, whilst the vertical walls are adiabatic. The Brinkman-Forchheimer-extended Darcy model has been used to describe the flow and heat transfer in the porous matrix. The governing equations in both flow domains, subject to a host of matching and boundary conditions, have been solved numerically. The results have been presented graphically and the influence of various transport parameters have been discussed.

AMS subject classification: 76R10, 76S99, 76D99.
Keywords: Composite system, Free convection, Brinkman-Forchheimer-extended Darcy model, ADI method.

[1]Corresponding author

1. Introduction

The theoretical and experimental investigations of simultaneous flows in a composite system made up of a clear region fluid overlying a fluid-saturated porous matrix have drawn attention of a large number of fluid dynamicists in the last few decades. This is primarily because of the wide-ranging applications of such studies in diverse areas from solidification of binary mixtures to migration of solutes in water saturated soils. Further applications commonly encountered in nature as well as in engineering are geophysical systems, electro-chemistry, fumigation of stored foodgrains, cooling of aluminium billets, and movement of moisture through air contained in fibrous insulation, to name a few, see, for instance, Straughan [1].

In the mathematical analyses of free convective flows involving fluid layers overlying a porous matrix, the basic model considered in the literature is that of Darcy law coupled with Beavers-Joseph slip condition at the clear region-porous region interface. On the other hand, for high permeability porous media, researchers have generally used the Brinkman extended Darcy model, often referred to as the Brinkman model, together with the continuity of velocities, shear stresses, heat fluxes, etc. at the interface [2–7]. Furthermore, a number of investigators have preferred a more general model, called Brinkman-Forchheimer-extended Darcy model [8–10]. This latter model is used to account for inertial terms, which assumes significance for flows with moderate to high velocities. In order to compare the relative merits of these models in composite flows involving porous media, Singh and Thorpe [11] have carried out a comparative analysis of them for natural convection in a vertical rectangular cavity containing an immiscible fluid layer adjoining a porous layer saturated with the same fluid.

The literature on natural convection in rectangular cavities and other geometries in the absence of mass transfer is quite exhaustive. The combined effects of heat and mass transfer on natural convection in rectangular enclosures have also been investigated by a number of scholars [12–14]. This type of convective flow is also known as double diffusive natural convection. As compared to the flows solely dominated by thermal buoyancy, double diffusive natural convection entails consideration of both heat and mass balance equations including their coupling with the momentum equations. When one considers the double diffusive convective flows in the presence of isotropic or anisotropic porous material, the mathematical analyses involving heat and mass transfer become more demanding due to the presence of two phases — clear fluid and the fully saturated porous matrix — necessitating the consideration of separate governing equations for each phase.

Nithiarasu *et al.* [15] have studied double diffusive free convective flow in a rectangular permeable cavity fully saturated with a viscous fluid. Applying the Brinkman-Forchheimer-extended Darcy model, numerical solution of double diffusive free convection in a composite cavity partially filled with a permeable material, has been discussed by Singh *et al.* [16]. Mahidjiba *et al.* [17] have used a finite element method to study numerically the onset of double diffusive convection in a horizontal porous cavity. The numerical study of Mohamad and Bennacer [18] deals with both two and three dimensional double diffusive convective flows in a horizontal porous cavity. They assumed

differentially heated walls of the cavity which is subjected to stably stratified species concentration imposed vertically. Some other features of double diffusive convective flows in rectangular enclosures fully or partially filled with porous material are anisotropy [19, 20], differentially salted species [21] and variable porosity [22]. Some other relevant works in double diffusive convective flows have been reported in [23–26]. Further aspects of natural convection in the presence of porous media, including surface chemical reaction and stability features, have been reported in [27–31].

In the present study, we have investigated natural convection in a vertical rectangular cavity partially occupied by an isotropic porous material. The system is subject to double diffusive convection due to the combined effects of horizontal thermal and concentration gradients. To model the flow in the porous region, we have used the Brinkman-Forchheimer-extended Darcy model. As stated earlier, the convective flow in this composite system is highly complex because of the nonlinearity and coupling of the governing conservation equations in the two regions. These equations have been solved numerically subject to a host of matching conditions at the fluid-porous medium interface as well as the boundary conditions on the impermeable walls of the cavity. The transport equations have been recast in terms of two derived variables — vorticity and stream function — to facilitate numerical integration using an ADI method. The governing equations and the associated boundary and matching conditions have been considered in nondimensional forms. We have solved the equations after first transforming them into parabolic form by addition of false transient term [32].

There are a number of nondimensional parameters that arise as part of the nondimensionalisation process. Of them, we have identified four key parameters — thermal Rayleigh number Ra, solutal Rayleigh number Rac, Darcy number Da and Lewis number Le — as central to our analysis. The effects of various processes described by these parameters have been discussed.

2. Mathematical formulation

As stated before, the composite system considered in this work consists of a viscous fluid layer (clear region) overlying a porous layer saturated with the same fluid, and occupying a vertical rectangular cavity of length L and height H, with impermeable boundaries. The physical configuration of the system is shown in Fig. 1. As shown therein, the x'-axis is taken in the horizontal direction and the y'-axis is taken in the vertical direction. The porous layer occupies the region $0 < y < H'_p$. The cavity is heated from below and cooled from above whilst the vertical boundaries are assumed to be insulated. Thus, we assume that the horizontal surfaces $y' = 0$ and $y' = H$ are maintained at constant temperatures T'_h and T'_c, respectively, and $T'_h > T'_c$ so that natural convection takes place in the cavity. The species concentrations at the surfaces $y' = 0$ and $y' = H$ are assumed to be C'_h and C'_c, respectively.

The fluid in the clear region is assumed to be incompressible with constant physical properties except density in the buoyancy force term in the momentum equation. Applying the Boussinesq approximation, we consider the density to be a linear function of the

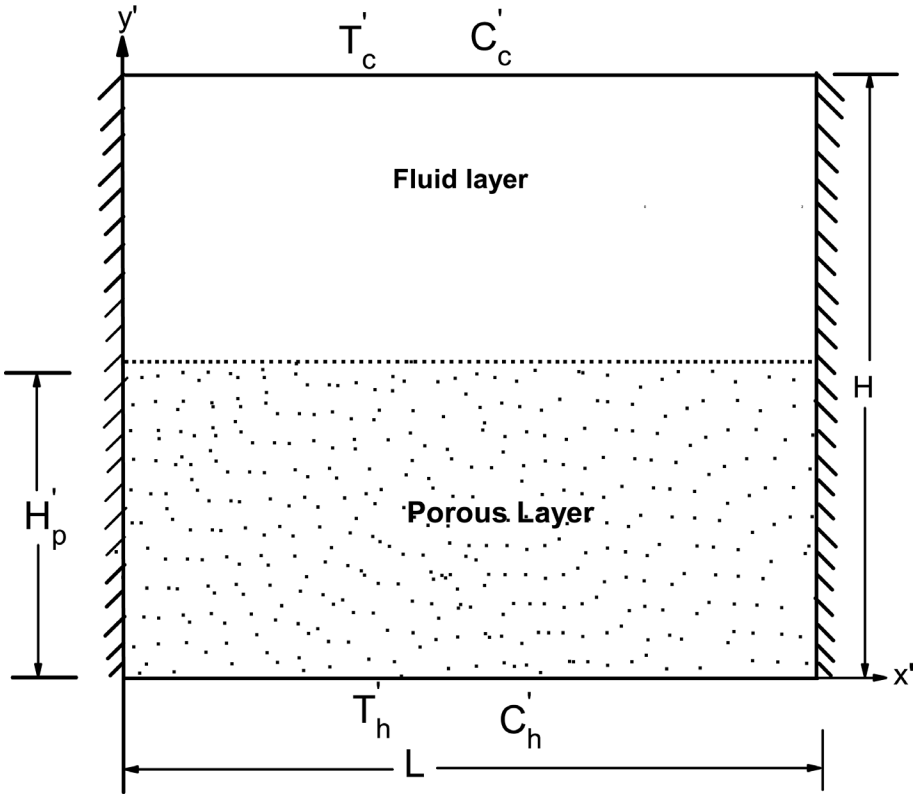

Figure 1: Physical configuration.

temperature and the species concentration. Furthermore, the porous layer is assumed to be homogeneous and isotropic. From the physical description above, it is obvious that the clear region and the porous region are separated by an interface which is assumed to be permeable so that flow takes place from one layer to the other. Such a physical situation necessitates the consideration of specific matching conditions on the velocity, shear stress, concentration and temperature at the interface besides the usual boundary conditions on the variables. We shall give these conditions after first presenting the governing equations of the system.

The equations governing the flow are the usual equations of continuity, momentum, energy and mass balance. A different set of equations govern the flow in each region. In the porous region, the flow is assumed to be governed by the Brinkman-Forchheimer-extended Darcy model. This model enables one to account for certain special nonlinear features of the flow. The equations are presented in terms of the vorticity component ζ' and stream function Ψ', defined by

$$u' = \frac{\partial \Psi'}{\partial y'}, \quad v' = -\frac{\partial \Psi'}{\partial x'} \tag{2.1}$$

$$\zeta' = \frac{\partial v'}{\partial x'} - \frac{\partial u'}{\partial y'} \tag{2.2}$$

where u' and v' are, respectively, the components of fluid velocity in the x' and y' directions. In view of Eqs (2.1) and (2.2), one can express the continuity and momentum equations in each region in terms of Ψ' and ζ'. The other equations relevant to our system are the diffusion equations governing the temperature and species concentration.

As is known, the governing equations for both regions constitute highly nonlinear coupled systems. In order to solve these equations numerically, and to analyse the heat and mass transfer characteristics, it is convenient if the equations and the corresponding boundary and matching conditions are presented in nondimensional forms. We thus introduce the nondimensional variables

$$\begin{aligned} (x,\ y) &= (x',\ y')/H\,, & (u,\ v) &= (H/\alpha_f)(u',\ v') \\ \zeta &= H^2\zeta'/\alpha_f\,, & \Psi &= \Psi'/\alpha_f \\ T &= (T' - T'_c)/(T'_h - T'_c)\,, & C &= (C' - C'_c)/(C'_h - C'_c) \end{aligned} \tag{2.3}$$

where α_f is the thermal diffusivity of the fluid.

Using Eq (2.3) in Eqs (2.1) and (2.2), we obtain

$$u = \frac{\partial \Psi}{\partial y}\,, \quad v = -\frac{\partial \Psi}{\partial x} \tag{2.4}$$

$$\zeta = \frac{\partial v}{\partial x} - \frac{\partial u}{\partial y} \tag{2.5}$$

Similarly, we can use Eq (2.3) together with the nondimensional porous region depth parameter $d = H'_p/H$ and the aspect ratio $\mathrm{Ar} = L/H$ in the (dimensional) governing equations in each region, which are not presented here, for brevity. In the following, the quantities with the suffix f refer to the clear region while those with the suffix p are for the porous region. The nondimensional equations for both regions can be obtained as [15]

Clear region ($0 \le x \le \mathrm{Ar}\,,\ d \le y \le 1$):

$$u_f \frac{\partial \zeta_f}{\partial x} + v_f \frac{\partial \zeta_f}{\partial y} = \mathrm{Pr}\left(\frac{\partial^2 \zeta_f}{\partial x^2} + \frac{\partial^2 \zeta_f}{\partial y^2}\right) + \mathrm{Ra}\,\mathrm{Pr}\,\frac{\partial T_f}{\partial x} + \mathrm{Rac}\,\mathrm{Pr}\,\frac{\partial C_f}{\partial x} \tag{2.6}$$

$$\frac{\partial^2 \Psi_f}{\partial x^2} + \frac{\partial^2 \Psi_f}{\partial y^2} = -\zeta_f \tag{2.7}$$

$$u_f \frac{\partial T_f}{\partial x} + v_f \frac{\partial T_f}{\partial y} = \frac{\partial^2 T_f}{\partial x^2} + \frac{\partial^2 T_f}{\partial y^2} \tag{2.8}$$

$$u_f \frac{\partial C_f}{\partial x} + v_f \frac{\partial C_f}{\partial y} = \frac{1}{\mathrm{Le}}\left(\frac{\partial^2 C_f}{\partial x^2} + \frac{\partial^2 C_f}{\partial y^2}\right) \tag{2.9}$$

Porous region ($0 \le x \le \mathrm{Ar},\ 0 \le y \le d$):

$$0 = \mathrm{Pr}\left(\frac{\partial^2 \zeta_p}{\partial x^2} + \frac{\partial^2 \zeta_p}{\partial y^2}\right) + \mathrm{Ra}\,\mathrm{Pr}\,\frac{\partial T_p}{\partial x} + \mathrm{Rac}\,\mathrm{Pr}\,\frac{\partial C_p}{\partial x} - \left(\frac{\mathrm{Pr}}{\mathrm{Da}} + \frac{F|V_p|}{\sqrt{\mathrm{Da}}}\right)\zeta_p - \frac{F}{\sqrt{\mathrm{Da}}}\left(v_p\frac{\partial |V_p|}{\partial x} - u_p\frac{\partial |V_p|}{\partial y}\right) \tag{2.10}$$

$$\frac{\partial^2 \Psi_p}{\partial x^2} + \frac{\partial^2 \Psi_p}{\partial y^2} = -\zeta_p \tag{2.11}$$

$$u_p\frac{\partial T_p}{\partial x} + v_p\frac{\partial T_p}{\partial y} = \lambda_1\left(\frac{\partial^2 T_p}{\partial x^2} + \frac{\partial^2 T_p}{\partial y^2}\right) \tag{2.12}$$

$$u_p\frac{\partial C_p}{\partial x} + v_p\frac{\partial C_p}{\partial y} = \frac{\lambda_2}{\mathrm{Le}}\left(\frac{\partial^2 C_p}{\partial x^2} + \frac{\partial^2 C_p}{\partial y^2}\right) \tag{2.13}$$

It may be mentioned that in deriving the above equations, we have assumed that the viscosity of the fluid in the clear region, μ_f, is equal to the viscosity of the fluid in the porous region, μ_p. This assumption has been reported in the literature to provide good agreement with experimental data [3, 33]. Of the undefined quantities appearing in Eqs (2.6), (2.8), (2.9), (2.10), (2.12) and (2.13), T is the temperature, C the species concentration, $V_p = \sqrt{u_p^2 + v_p^2}$ and F is the inertia coefficient. The parameter F can be evaluated using an empirical formula [11, 34], $F = 0.05\sqrt{7}\epsilon^{-3/2}$, where ϵ is the porosity of the medium. For instance, in the case of a porous medium composed of spherical beads ($0.35 \le \epsilon \le 0.45$), F is approximately equal to 0.52 when $\epsilon = 0.4$.

The nondimensionalisation of the equations has given rise to a number of well-known nondimensional parameters. The parameters appearing in Eqs (2.6), (2.9), (2.10), (2.12) and (2.13) are the Prandtl number Pr, Darcy number Da, ratio λ_1 of the thermal conductivities the porous and fluid layers, ratio λ_2 of the mass diffusivities of the porous and fluid layers, thermal Rayleigh number Ra, solutal Rayleigh number Rac and the Lewis number Le. These are defined as

$$\mathrm{Pr} = \frac{\nu_f}{\alpha_f}, \quad \mathrm{Da} = \frac{K}{H^2}, \quad \lambda_1 = \frac{\kappa_p}{\kappa_f}, \quad \lambda_2 = \frac{D_p}{D_f}$$
$$\mathrm{Le} = \frac{\alpha_f}{D_f}, \quad \mathrm{Ra} = \frac{g\beta H^3(T_h' - T_c')}{\alpha_f \nu_f}, \quad \mathrm{Rac} = \frac{g\beta^* H^3(C_h' - C_c')}{\alpha_f \nu_f} \tag{2.14}$$

where ν is the kinematic viscosity, K the permeability of the porous medium, D the mass diffusivity, g the acceleration due to gravity, β the coefficient of thermal expansion, β^* the coefficient of concentration expansion, and κ is the thermal conductivity of the fluid.

2.1. Boundary and matching conditions

The boundary conditions applicable to the present problem are

$$\frac{\partial T}{\partial x} = \frac{\partial C}{\partial x} = 0 \ \text{ on } \ x = 0, \ \ \mathrm{Ar} \tag{2.15}$$

$$T = C = 1 - y \quad \text{on} \quad y = 0, \quad y = 1 \tag{2.16}$$

$$\Psi = 0 \quad \text{on} \quad x = 0, \quad \text{Ar} \quad \text{and} \quad y = 0, \ 1 \tag{2.17}$$

$$\zeta = -\frac{\partial^2 \Psi}{\partial x^2} \quad \text{on} \quad x = 0, \quad x = \text{Ar} \tag{2.18}$$

$$\zeta = -\frac{\partial^2 \Psi}{\partial y^2} \quad \text{on} \quad y = 0, \quad y = 1 \tag{2.19}$$

The matching conditions at the clear region-porous medium interface $y = d$, by assuming the continuity of temperature, heat flux, concentration and concentration flux are

$$T_f = T_p\,, \quad \frac{\partial T_f}{\partial y} = \lambda_1 \frac{\partial T_p}{\partial y} \quad \text{on} \quad y = d \tag{2.20}$$

$$C_f = C_p\,, \quad \frac{\partial C_f}{\partial y} = \lambda_2 \frac{\partial C_p}{\partial y} \quad \text{on} \quad y = d \tag{2.21}$$

The matching conditions on the vorticity and stream function cannot be specified directly, and must be derived from the matching conditions of the velocity and shear stress components at the interface. After some mathematical manipulations these conditions can be derived as

$$\zeta_f = \zeta_p\,, \quad \frac{\partial \zeta_f}{\partial y} = \frac{\partial \zeta_p}{\partial y} \quad \text{on} \quad y = d \tag{2.22}$$

$$\Psi_f = \Psi_p\,, \quad \frac{\partial \Psi_f}{\partial y} = \frac{\partial \Psi_p}{\partial y} \quad \text{on} \quad y = d \tag{2.23}$$

3. Numerical procedure

The problem modelled mathematically in Section 2 is governed by nonlinear coupled differential equations and this suggests that solutions of the equations must be obtained numerically. The false transient method described in detail by Mallinsion and de Vahl Davis [32] is used to solve numerically the transformed equations in parabolic form. The transport equations are discretised on a uniform grid and the resulting finite difference equations are solved by the alternating direction implicit (ADI) method proposed by Samarskii and Andreyev [35]. This method, as claimed by Mallinson and de Vahl Davis [32], has some advantage in comparison to the original ADI scheme of Peaceman and Rachford [36] for the solution of two-dimensional problems. The numerical integration for each dependent variable in both regions is processed using standard procedures. The marching scheme for the numerical integration, and the application of matching conditions at the interface follow closely the procedure reported in literature, see *e.g.,* [11], and are not repeated here.

In the process of iteration, using the initial values of the temperature, concentration and velocity components, the temperature and concentration fields are computed first and then the vorticity and the stream functions are evaluated. In the last stage, the

velocity components are obtained by employing the newly obtained stream function. The solution process from the initial state is iterated until the steady-state solution is obtained by satisfying the following convergence criterion with respect to each variable:

$$\frac{\sum_i \sum_j \left| \tau_{i,j}^{n+1} - \tau_{i,j}^{n} \right|}{m|\tau|_{\max}} < \tau_{\text{err}} \tag{3.1}$$

where m is the number of interior grid points, $|\tau|_{\max}$ the maximum magnitude of τ, τ_{err} a pre-determined maximum error criterion determined by numerical experiments, and τ may represent temperature or concentration or vorticity or stream function. The superscripts, as indicated, denote the values of the dependent variables after the nth and $(n+1)$th iterations. The indices i and j indicate the grid locations in the (x, y)-plane. In the numerical computations, corresponding to the values of Ra equal to 10^4 and 10^5, we set τ_{err} at 5×10^{-5} while for 10^6, it was set at 5×10^{-4} because of the large number of iterations required to satisfy the convergence criterion and also because of the slightly oscillatory nature of the solution due to the coupling of the governing equations.

Extensive numerical tests were performed in order to check the validity of the numerical code. A detailed description of these tests is described in [11]. The accuracy of the numerical code was also validated by comparing the results with the published work of Nishimura *et al.* [37]. Convergence of the numerical method was investigated by carrying out experiments on 21×21 to 101×101 uniform grids. It was seen that a finer mesh size produced better results and thus, the solution has been obtained using uniformly spaced 101×101 grid points in all the cases.

Two quantities of practical interest in the present problem are the Nusselt number Nu, and the Sherwood number Sh. The local Nusselt number at the heated surface is given by

$$\text{Nu}(x) = -\lambda_1 \frac{\partial T_p}{\partial y} \tag{3.2}$$

and the average Nusselt number on the heated surface is

$$\text{Nu}_{\text{av}} = \frac{1}{\text{Ar}} \int_0^{\text{Ar}} \text{Nu}(x)\, \text{d}x \tag{3.3}$$

Similarly, we define the average Sherwood number as

$$\text{Sh}_{\text{av}} = \frac{1}{\text{Ar}} \int_0^{\text{Ar}} \text{Sh}(x)\, \text{d}x \tag{3.4}$$

where

$$\text{Sh}(x) = -\lambda_2 \frac{\partial C_p}{\partial y} \tag{3.5}$$

One can obtain the average Nusselt number and the average Sherwood number at the cooled surface in the same way as above. It is observed that the differences between average values obtained at the two walls are within 0.5% which is an indication of convergence as well as correctness of our numerical code.

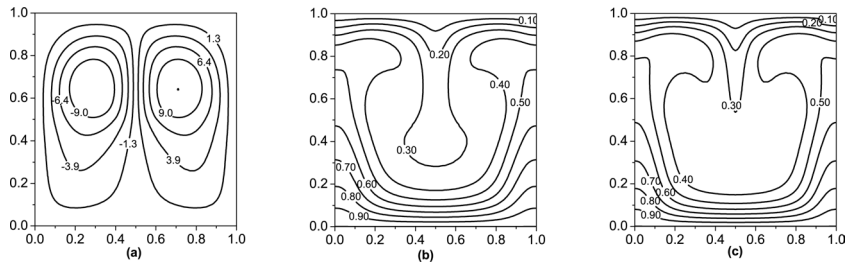

Figure 2: (a) Streamlines (b) Isotherms (c) Isosolutes
$\mathrm{Ra} = 10^5,\ \mathrm{Rac} = 10^5,\ \mathrm{Da} = 10^{-3},\ \mathrm{Le} = 1.47.$

4. Results and discussion

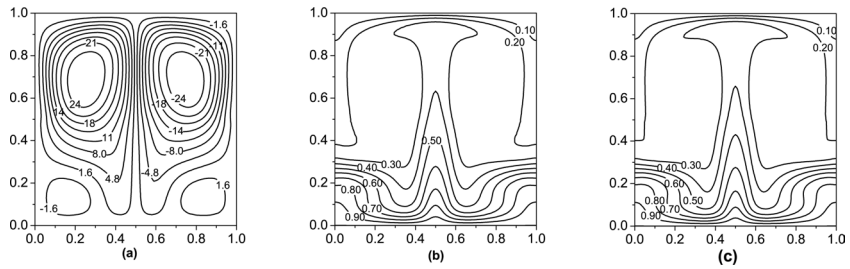

Figure 3: (a) Streamlines (b) Isotherms (c) Isosolutes
$\mathrm{Ra} = 10^6,\ \mathrm{Rac} = 10^5,\ \mathrm{Da} = 10^{-3},\ \mathrm{Le} = 1.18$

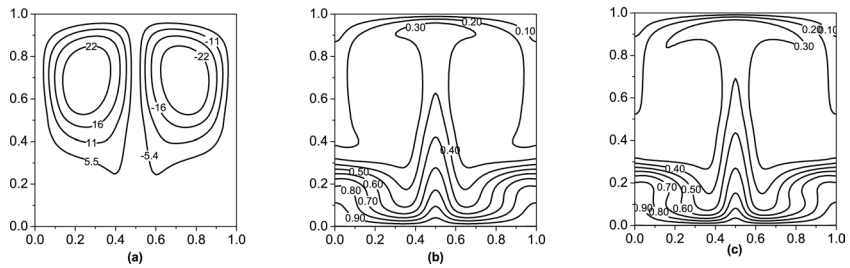

Figure 4: (a) Streamlines (b) Isotherms (c) Isosolutes
$\mathrm{Ra} = 10^6,\ \mathrm{Rac} = 10^5,\ \mathrm{Da} = 10^{-3},\ \mathrm{Le} = 1.47$

As seen in Section 2, the composite natural convective flow being considered in this work is governed by a large number of nondimensional parameters. As a consequence, it is possible to visualize a huge variety of typical flows within the confines of the cavity by varying one or more of these parameters while keeping others fixed. However, this is a highly formidable task. For the purpose of this study, we have identified some key parameters of our interest. As indicated earlier, we have chosen Ra and Rac –

representing two buoyancy forces resulting from the differentials in the temperature and species concentration, respectively, at the lower and upper walls of the enclosure; Le – the ratio of viscous diffusivity and mass diffusivity; and Da – representing the permeability of the porous medium. We shall thus focus our attention in analyzing graphically the effects of variation in these important transport parameters on physical quantities such as streamlines, isotherms, isosolutes (Figs. 2–7), vertical component of velocity, temperature and concentration profiles at the clear fluid-porous region interface (Figs. 8–10) and local Nusselt number and local Sherwood number (Figs. 11–12). The remaining parameters occurring in our analysis have been assigned the fixed values: Ar $= 1.0$, Pr $= 0.71$, $d = 0.5$, $\lambda_1 = 1.0$ and $\lambda_2 = 1.0$. We are thus effectively looking at the composite flow in a square cavity occupied equally by clear and porous layer fluids. Before analyzing in detail various illustrations, it is worth mentioning that the physical configuration being considered presently — lower and upper boundaries of the cavity being subjected to differential constant temperatures and species concentrations while sidewalls being adiabatic with regard to thermal and mass transfer — has received comparatively much less attention in the literature, to the authors' knowledge. Thus, the graphical results presented and discussed below assume more significance due to their observed special patterns, particularly symmetry of typical contours.

In Fig. 2, we have shown the streamlines, isotherms and isosolutes for Ra $= 10^5$, Rac $= 10^5$, Da $= 10^{-3}$ and Le $= 1.47$. Most interestingly, as mentioned above, we observe symmetry of these contours about the centre line of the cavity at $x = 0.5$, particularly noting the formation of two loops for the streamlines on either side of the central vertical line. It needs to be pointed out at this early stage that such symmetry features will remain the hallmark of various contour illustrations that will follow in the other figures. Coming back to this figure, we first note from the streamline loops that the heated fluid moves clockwise on the left loop and anti-clockwise on the right loop. Thus the fluid rises along either vertical wall, and falls down in the middle region as a result of cooling taking place at the upper wall. The effects of the higher temperature and higher concentration of solutes at the lower wall bounding the porous medium are apparently visible in the contours representing isotherms and isosolutes. Both these contours exhibit similar profiles. In the next Fig. 3, we have shown patterns of streamlines, isotherms and isosolutes for Ra $= 10^6$, Rac $= 10^5$, Da $= 10^{-3}$ and Le $= 1.18$. Interestingly, streamlines show boundary layer type phenomenon, particularly in the clear region of the cavity, besides formation of two additional symmetric loops near the adiabatic walls in the porous region. Furthermore, the similarity of the profiles of isotherms and isosolutes, observed earlier in Fig. 2, is more pronounced here, and they in fact become nearly identical. In order to assess the effect of change in Ra, keeping the remaining three parameters fixed, we have included streamlines, isotherms and isosolutes for Ra $= 10^6$, Rac $= 10^5$, Da $= 10^{-3}$ and Le $= 1.47$ in Fig. 4. A comparison of contours in Figs. 2 and 4 clearly indicates the extent and scope of the changes brought about by increasing Ra from 10^5 to 10^6. Firstly, the streamlines are pushed significantly towards the clear region of the cavity. Secondly, both isotherms and isosolutes in the two cases show quite a distinct profile pattern, with an increase in the thermal Rayleigh number.

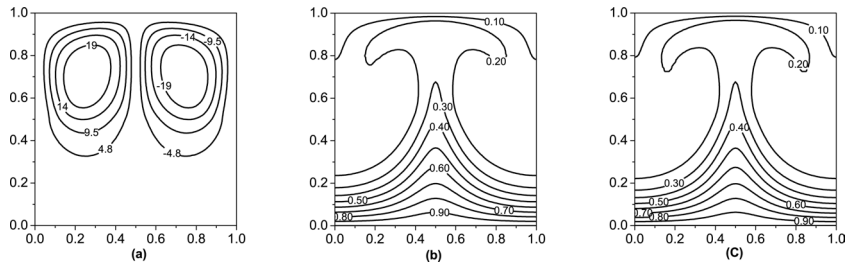

Figure 5: (a) Streamlines (b) Isotherms (c) Isosolutes
$\mathrm{Ra} = 10^6,\ \mathrm{Rac} = 10^5,\ \mathrm{Da} = 10^{-6},\ \mathrm{Le} = 1.18$

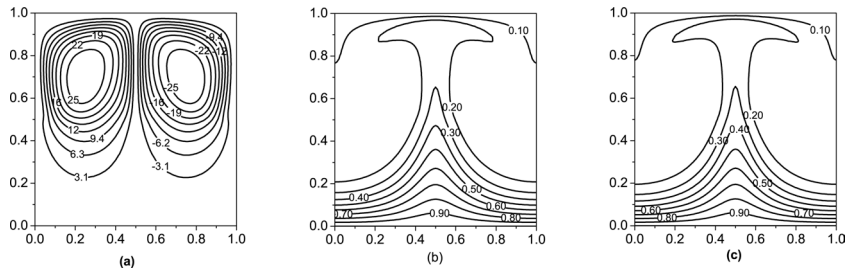

Figure 6: (a) Streamlines (b) Isotherms (c) Isosolutes
$\mathrm{Ra} = 10^6,\ \mathrm{Rac} = 10^6,\ \mathrm{Da} = 10^{-6},\ \mathrm{Le} = 1.18$

The next three figures correspond to a lower porous medium region whose permeability is much smaller as compared to the previous three figures. Fig. 5 illustrates typical contours for $\mathrm{Ra} = 10^6$, $\mathrm{Rac} = 10^5$, $\mathrm{Da} = 10^{-6}$ and $\mathrm{Le} = 1.18$. By comparing the corresponding profiles in the Figs. 3 and 5, one can easily gauge the effect of change in the permeability of the porous medium. There is a striking contrast in the pattern of streamlines for $\mathrm{Da} = 10^{-3}$ versus $\mathrm{Da} = 10^{-6}$ cases; apparently, as a result of increase in the permeability of the porous medium (cf. streamlines in Fig. 3), there is larger fluid motion in the porous region and hence higher intensity of free convection currents. Even the isotherms and isosolutes, particularly in the lower porous region, show a distinct pattern as a result of such a change in the value of Da. The contours depicted in the next

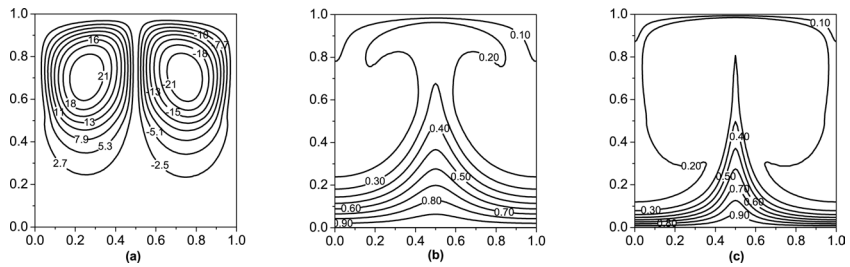

Figure 7: (a) Streamlines (b) Isotherms (c) Isosolutes
$\mathrm{Ra} = 10^6,\ \mathrm{Rac} = 10^5,\ \mathrm{Da} = 10^{-6},\ \mathrm{Le} = 7.0$

Fig. 6 have been drawn for Ra = Rac = 10^6, Da = 10^{-6} and Le = 1.18. By comparing Figs. 5 and 6, we can notice that a change in the value of the solutal Rayleigh number while, as usual, keeping other three parameters fixed, does indeed have its impact on the pattern of fluid circulation, *i.e.*, streamlines, in the enclosure. However, isotherms and isosolutes are seemingly little affected by such an increase in Rac. In the last set of contours (Fig. 7), we have presented contour graphs by choosing Ra = 10^6, Rac = 10^5, Da = 10^{-6} and Le = 7.0, apparently to assess the effect of the parameter Le. Figures 5 and 7 allow us to estimate the switch in the transport processes due to a relative big jump in the Lewis number. Notably, streamlines get significantly denser, although as expected on the physical grounds, most circulation continues to take place in the clear region of the cavity space. Furthermore, one can easily notice the insensitivity of isotherms to such a change in the Lewis number. However, it needs to be pointed out that isosolutes do get modified by increase in the value of Le which is physically expected due to the very definition of the Lewis number. To sum up the effects of Ra and Rac on the level curves for the stream function, temperature and concentration, we notice from a comparison of Fig. 2 with the other Figs. 3–7, that as either of Ra or Rac is increased from 10^5 to 10^6, the fluid circulation changes from clockwise to anticlockwise or vice versa. Furthermore, the isotherms and isosolutes also change their patterns with increase in the thermal or solutal Rayleigh numers, as already pointed out before. These contrasting features apply to high as well as low permeability porous media.

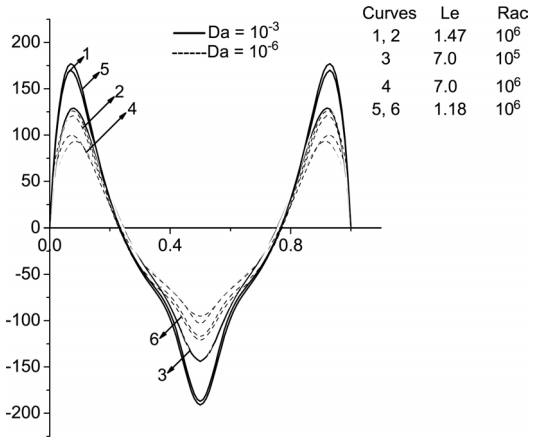

Figure 8: Velocity component v at the interface. Ra = 10^6

In the next set of three illustrations (Figs. 8–10), we have shown some representative profiles of vertical component of velocity, temperature and concentration, respectively, at the clear region-porous medium interface of the cavity. Figure 8 exhibits variation of the vertical component of velocity across the cavity in the horizontal direction for Ra = 10^6, by considering sets of combinations of the parameters Da, Le and Rac. It is interesting to note that the negative peak values of this component of velocity in the central part are larger in magnitude in comparison to the positive peak values occurring close to the adiabatic vertical walls. Moreover, there is an apparent amplification in the

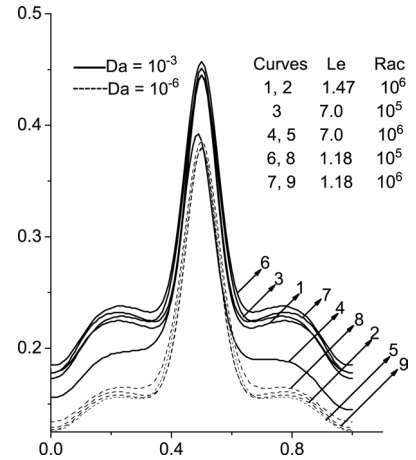

Figure 9: Temperature profiles at the interface. Ra $= 10^6$

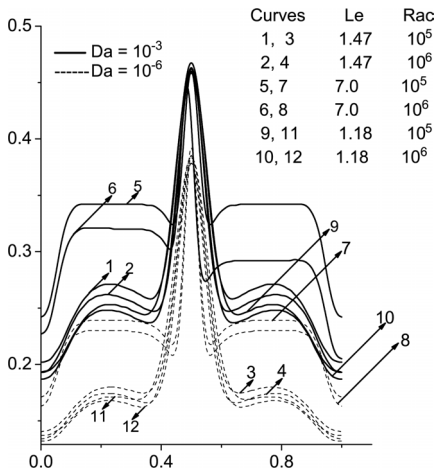

Figure 10: Concentration profiles at the interface. Ra $= 10^6$

flow with increase of the Darcy number from 10^{-6} to 10^{-3}. The vertical component of velocity also shows more variations for larger values of the Darcy number. The variation of temperature when Ra $= 10^6$, has been depicted in the profiles shown in the Fig. 9. Here, we have included as many as nine profiles corresponding to a range of combinations of the Darcy number, solutal Rayleigh number and Lewis number, as in the case of vertical velocity. The fluid temperature apparently has its peak in the very central portion of the interface and shows its upward bias with increasing Darcy number. In the next Fig. 10, we have illustrated a number of concentration profiles when Ra $= 10^6$, while varying other transport parameters as in the cases of velocity and temperature above. Interestingly, the concentration profiles are broadly similar to the temperature profiles in the central as well as other portions of the horizontal interface. However, the temperature profiles show a certain degree of deviation from the concentration profiles corresponding to some specific combinations of the parameters Le, Rac and Da in that

while the former profiles appear to vary very little on either side of the middle region, the latter ones exhibit relatively larger variations.

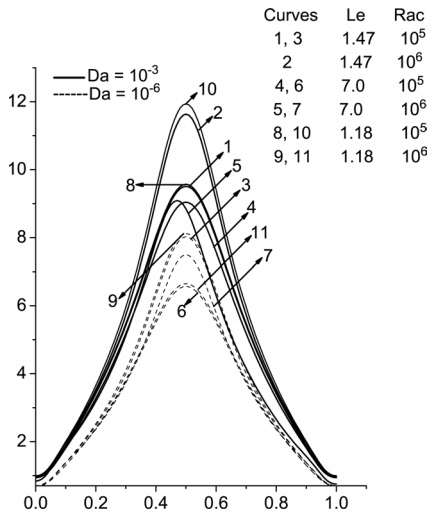

Figure 11: Local Nusselt number at $y = 0$. $\mathrm{Ra} = 10^6$

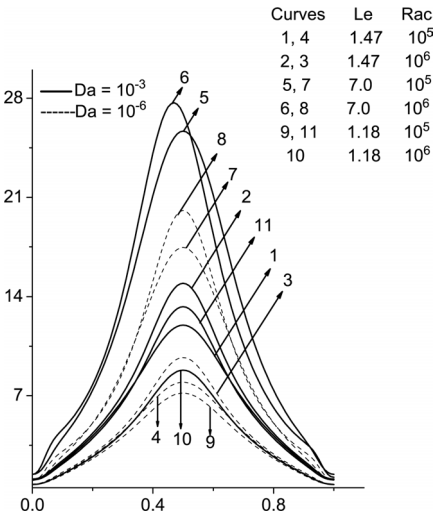

Figure 12: Local Sherwood number at $y = 0$. $\mathrm{Ra} = 10^6$

In order to get a further insight into the double diffusive natural convection being investigated here, we have examined the horizontal variation of local Nusselt number and local Sherwood number representing, respectively, heat and mass transfers. The variation of these quatities can be shown at the hot as well as the cold horizontal boundaries of the cavity. However, for illustrative purposes, we have shown here the variations of $\mathrm{Nu_{av}}$ and $\mathrm{Sh_{av}}$ on the warmer boundary $y = 0$ only. The profiles of the local Nusselt number have been shown in Fig. 11 and those of local Sherwood number in Fig. 12. It is seen

that the heat transfer at the warmer bottom boundary follow parabolic profiles, and the curves attain their maxima near its central portion, for all parameter values considered. A similar observation holds for the horizontal variation of the local Sherwood number. The individual effects of Da, Le and Rac on the local Nusselt and Sherwood numbers can also be gauged from these figures. In particular, it is interesting to note the increased heat and mass transfers at the warmer boundary with an increase in the permeability of the porous layer.

Table 1: Numerical values of $\mathrm{Nu_{av}}$ and $\mathrm{Sh_{av}}$ at $y = 0$ $\mathrm{Pr} = 0.71$

Ra	Rac	Da	Le	$\mathrm{Nu_{av}}$	$\mathrm{Sh_{av}}$
10^5	10^5	10^{-6}	1.18	3.0818	3.3057
			1.47	3.0229	3.5616
		10^{-3}	1.18	3.3097	3.5846
			1.47	3.2912	3.9581
	10^6	10^{-6}	1.18	3.2670	3.5035
			1.47	3.1412	3.6966
		10^{-3}	1.18	4.6131	5.0877
			1.47	4.3318	5.4734
10^6	10^5	10^{-6}	1.18	3.3566	3.6019
			1.47	3.3466	3.9515
		10^{-3}	1.18	4.8168	5.2922
			1.47	4.7827	5.9335
	10^6	10^{-6}	1.18	3.7709	4.0570
			1.47	3.6996	4.3915
		10^{-3}	1.18	5.4961	6.0700
			1.47	5.3214	6.7032

In order to further assess the effect of the nondimensional parameters on the heat and mass transfers, we have computed the average values of the Nusselt and Sherwood numbers on $y = 0$. These are given in Table 1. As stated before, $\mathrm{Nu_{av}}$ and $\mathrm{Sh_{av}}$ indicate, respectively, estimates of the overall heat and mass transfer rates at the boundary. Based on the numerical values given in Table 1, we make the following observations:

(a) For fixed values of Ra, Rac and Da, the average Sherwood number increases while the average Nusselt number decreases as the Lewis number increases. In other words, near the warmer bottom boundary of the cavity, an increase in the Lewis number results in an increase in the thermal boundary layer and a decrease in the concentration boundary layer.

(b) The average Nusselt number is less than the average Sherwood number for the values of Le considered here. This indicates that the heat transfer at the warmer

bottom boundary is less than the mass transfer when thermal diffusion is less than or nearly equal to the mass diffusion.

(c) Both quantities $\mathrm{Nu}_{\mathrm{av}}$, and $\mathrm{Sh}_{\mathrm{av}}$ increase as the Darcy number Da increases. Thus, as the permeability of the porous layer increases, the overall heat and mass transfers at the warmer boundary increase which, in turn, leads to the formation of thinner thermal and concentration boundary layers.

(e) The effects of thermal and solutal Rayleigh numbers are similar to that of the Darcy number. As Rac and Ra are increased, the quantities $\mathrm{Nu}_{\mathrm{av}}$, and $\mathrm{Sh}_{\mathrm{av}}$ also increase indicating the positive influence of larger thermal and concentration buoyancy forces on enhancing the heat and mass transfers.

5. Conclusions

Effects of buoyancy, permeability and mass transfer have been analyzed for a double diffusive natural convective flow in a rectangular cavity half-filled with a highly permeable porous material. These processes have been parametrized by four key quantities — Lewis number, thermal and solute Rayleigh numbers, and Darcy number. It is assumed that the upper and lower boundaries of the cavity are maintained at different temperatures and species concentrations, while the side walls are adiabatic. The governing equations have been solved numerically using an ADI method. The solutions have been presented graphically for streamlines, isotherms, isosolutes, velocity, temperature and concentration. We have also shown variations of local Nusselt and Sherwood numbers.

Nomenclature

Ar	aspect ratio, L/H
C	nondimensional species concentration
d	nondimensional porous region depth parameter, H'_p/H
D	mass diffusivity
Da	Darcy number
F	inertia coefficient in the Brinkman-Forchheimer-extended Darcy model
g	acceleration due to gravity
H	height of the enclosure
K	permeability of the porous medium
L	length of the enclosure
Le	Lewis number
$\mathrm{Nu}_{\mathrm{av}}$	average Nusselt number
$\mathrm{Nu}(x)$	local Nusselt number
Pr	Prandtl number
Ra	thermal Rayleigh number
Rac	solutal Rayleigh number

$\mathrm{Sh}_{\mathrm{av}}$	average Sherwood number
$\mathrm{Sh}(x)$	local Sherwood number
T	nondimensional temperature
$u,\ v$	nondimensional velocity components
$x,\ y$	nondimensional coordinates

α	thermal diffusivity
β	coefficient of thermal expansion
β^*	coefficient of concentration expansion
ϵ	porosity
κ	thermal conductivity
λ_1	ratio of thermal conductivities of porous and fluid layers
λ_2	ratio of mass diffusivities of porous and fluid layers
ψ	nondimensional stream function
μ	viscosity
ν	kinematic viscosity
ζ	nondimensional vorticity

Subscripts

c	cold wall
f	fluid layer
h	hot wall
p	porous layer

Note : Primed symbols denote the corresponding dimensional quantities

References

[1] Straughan, B., 2008, Stability and Wave Motion in Porous Media, Appl. Math. Sci. Ser., Springer, New York.

[2] Trevisan, O.V., and Bejan, A., 1987, "Combined heat and mass transfer by natural convection in a vertical enclosure", ASME J. Heat Transf., 109, pp. 104–112.

[3] Neale, G., and Nader, W., 1974, "Practical significance of Brinkman's extension of Darcy's law: Coupled parallel flows within a channel and a bounding porous medium", Can. J. Chem. Engng., 52, pp. 475–478.

[4] Sacheti, N. C., and Bhatt, B. S., 1988, "Stokes and Rayleigh layers in presence of naturally permeable boundaries", in: P.N. Cheremisionoff, N.P. Cheremisionoff (Eds.), Civil Engineering Practice 2, Technomic Publ., Lancaster, USA, pp. 659–695.

[5] Bhatt, B. S., and Sacheti, N. C., 1994, "Flow past a porous spherical shell using the Brinkman model", J. Phys. D: Appl. Phys., 27, pp. 37–41.

[6] Payne, L. E., and Straughan, B., 1998, "Analysis of boundary condition at the interface between a viscous fluid and a porous medium and related modeling questions", J. Math. Pures Appl., 77, pp. 317–354.

[7] Straughan, B., 2002, "Effect of property variation and modelling on convection in a fluid overlying a porous layer", Int. J. Numer. Anal. Meth. Geomech., 26, pp. 75–97.

[8] Beckermann, C., Ramadhyani, S., and Viskanta, R., 1987, "Natural convection flow and heat transfer between a fluid layer and a porous layer inside a rectangular enclosure", ASME J. Heat Transf., 109, pp. 363–370.

[9] Beckermann, C., Viskanta, R., and Ramadhyani, S., 1988, "Natural convection in a vertical enclosure containing simultaneously fluid and porous layers", J. Fluid Mech., 186, pp. 257–286.

[10] Payne, L. E., and Straughan, B., 1999, "Convergence, continuous dependence and decay for the Brinkman-Forchheimer equations", Stud. Appl. Math., 102, pp. 419–439.

[11] Singh, A. K., and Thorpe, G. R., 1995, "Natural convection in a confined fluid overlying a porous layer–A comparison study of different models", Indian J. Pure Appl. Math., 26, pp. 81–95.

[12] Wee, H. K., Keey, R. B., and Cunningham, M. J., 1989, "Heat and moisture transfer by natural convection in a rectangular cavity", Int. J. Heat Mass Transf., 32, pp. 1765–1778.

[13] Kazmierczak, M., and Poulikakos, D., 1990, "Transient double diffusion in a stably stratified fluid layer heated from below", Int. J. Heat Fluid Flow, 11, pp. 30–39.

[14] Han, H., and Kuehn, T. H., 1991, "Double diffusive natural convection in a vertical rectangular enclosure–II. Numerical study", Int. J. Heat Mass Transf., 34, pp. 461–471.

[15] Nithiarasu, P., Sundararajan, T., and Seetharamu, K. N., 1997, "Double-diffusive natural convection in a fluid saturated porous cavity", Int. Comm. Heat Mass Transf., 24, pp. 1121–1130.

[16] Singh, A. K., Paul, T., and Thorpe, G. R., 1999, "Natural convection due to heat and mass transfer in a composite system", Heat Mass Transf., 35, pp. 39–48.

[17] Mahidjiba, A., Mamou, M., and Vasseur, P., 2000, "Onset of double diffusive convection in a rectangular porous cavity subject to mixed boundary conditions", Int. J. Heat Mass Transf., 43, pp. 1505–1522.

[18] Mohamad, A. A., and Bennacer, R., 2002, "Double diffusion, natural convection in an enclosure filled with saturated porous medium subjected to cross gradients; stably stratified fluid", Int. J. Heat Mass Transf., 45, pp. 3725–3740.

[19] Bera, P., and Khalili, A., 2002, "Double-diffusive natural convection in an anisotropic porous cavity with opposing buoyancy forces: multi-solutions and oscillations", Int. J. Heat Mass Transf., 45, pp. 3205–3222.

[20] Gaikwad, S. N., Malashetty, M. S., and Prasad, K. R., 2009, "An analytical study of linear and nonlinear double diffusive convection in a fluid saturated anisotropic porous layer with Soret effect", Appl. Math. Model., 33, pp. 3617–3635.

[21] Bourich, M., Hasnaoui, M., and Amahmid, A., 2004, "Double-diffusive natural convection in a porous enclosure partially heated from below and differentially salted", Int. J. Heat Fluid Flow, 25, pp. 1034–1046.

[22] Akbal, S., and Bayta, F., 2008, "Effects of non-uniform porosity on double diffusive natural convection in a porous cavity with partially permeable wall", Int. J. Thermal Sci., 47, pp. 875–885.

[23] Gobin, D., Goyeau, B., and Neculae, A., 2005, "Convective heat and solute transfer in partially porous cavities", Int. J. Heat Mass Transf., 48, pp. 1898–1908.

[24] Hill, A. A., 2005, "Double diffusive convection in a porous medium with a concentration based internal heat source", Proc. R. Soc. Lond. A, 461, pp. 561–574.

[25] Malashetty, M. S., Swamy, M., and Heera, R., 2008, "Double diffusive convection in a porous layer using a thermal non-equilibrium model", Int. J. Thermal Sci., 47, pp. 1131–1147.

[26] Malashetty, M. S., and Biradar, B. S., 2011, "The onset of double diffusive reaction-convection in an anisotropic porous layer", Phys. Fluids, 23, 064102.

[27] Straughan, B., 2006, "Global nonlinear stability in porous convection with a thermal non-equilibrium model", Proc. R. Soc. Lond. A, 462, pp. 409–418.

[28] Hill, A. A., 2009, "A differential constraint approach to obtain global stability for radiation-induced double-diffusive convection in a porous medium", Math. Meth. Appl. Sci., 32, pp. 914–921.

[29] Postelnicu, A., 2009, "Onset of convection in a horizontal porous layer driven by catalytic surface reaction on the lower wall", Int. J. Heat Mass Transf., 52, pp. 2466–2470.

[30] Scott, N. L., and Straughan, B., 2011, "Convection in a porous layer with a surface reaction", Int. J. Heat Mass Transf., 54, pp. 5653–5657.

[31] Tiwari, A. K., Singh, A. K., Chandran, P., and Sacheti, N. C., 2012, "Natural convection in a cavity with a sloping upper surface filled with an anisotropic porous material", Acta Mech., 223, pp. 95–108.

[32] Mallinson, G., and de Vahl Davis, G., 1973, "The method of false transient for the solution of coupled differential equations", J. Comp. Phys., 12, pp. 435–461.

[33] Lundgren, T. S., 1972, "Slow flow through stationary random beds and suspensions of spheres", J. Fluid Mech., 51, pp. 273–299.

[34] Ergun, S., 1952, "Fluid flow through packed columns", Chem. Engng. Progr., 48, pp. 89–94.

[35] Samarskii, A. A., and Andreyev, V. B., 1963, "On a high-accuracy difference scheme for an elliptic equation with several space variables", USSR J. Comp. Math. Math. Phys., 3, pp. 1373–1382.

[36] Peaceman, D. W., and Rachford, D. D., 1955, "The natural solution of parabolic and elliptic differential equations", J. Soc. Ind. Appl. Math., 3, pp. 28–47.

[37] Nishimura, T., Takumi, T., Shiraishi, M., Kawamura, Y., and Ozoe, H., 1986, "Numerical analysis of natural convection in a rectangular enclosure horizontally divided into fluid and porous regions", Int. J. Heat Mass Transf., 29, pp. 889–898.